IOP Publishing Measurement Science and Technology
Meas. Sci. Technol. **34** (2023) 025012 (11pp) https://doi.org/10.1088/1361-6501/ac9540

A localization method for subsea pipeline based on active magnetization

Xinjing Huang, Yuan Wang, Jinyu Ma, Jialin Wu, Jian Li, Yu Zhang and Hao Feng*

State Key Laboratory of Precision Measuring Technology and Instruments, Tianjin University, Tianjin, People's Republic of China

E-mail: fenghao@tju.edu.cn

Received 12 August 2022
Accepted for publication 27 September 2022
Published 10 November 2022

Abstract

Accurate location of subsea pipelines is a prerequisite for real-time tracking and detailed inspections by underwater robots. The magnetic anomalies generated by ferromagnetic pipelines can be used to locate both exposed and buried pipelines. However, due to the low signal ratio and model inconsistencies under weak and variable ambient magnetization, there is currently no intuitive and reliable pipeline detection method for pipeline tracking. This paper proposes a method capable of immediately and accurately locating pipelines via active magnetization and vertical magnetic measurements. Finite element simulations show that a magnet array can significantly enhance the magnetic anomaly, and that the vertical magnetic component alone can accurately indicate the pipeline's position, avoiding the inconvenience of magnetic three-component alignment in the field. It is experimentally demonstrated that the magnetic detection signal-to-noise ratio can be significantly increased by 5 dB–20 dB for a Φ219 mm steel pipe using the magnet array, and the maximum lateral positioning error is 0.03 m and much smaller than that without the magnet array.

Keywords: subsea pipeline, localization, magnetic field, magnetization

(Some figures may appear in colour only in the online journal)

1. Introduction

Subsea oil and gas pipelines have to work in harsh environments over a long time. As corrosion and aging develop, the risk of pipeline rupture becomes higher and higher. If a subsea pipeline leaks, it will cause very severe economic losses and environmental pollution. Regular inspection and monitoring of subsea pipelines are of great importance to ensure safe transportation of oil and gas. Employment of smart underwater robots, such as autonomous underwater vehicles (AUVs) and remotely operated vehicles (ROVs), for autonomous tracking, defect inspection and maintenance of subsea pipelines is becoming more and more popular, and has gradually become a new pipeline operation standard [1, 2]. Precise detection of subsea pipelines is not only a prerequisite for real-time tracking but also for defect inspection and pipeline maintenance. Since subsea pipelines are underwater or buried, underwater robots need a variety of sensors, such as sonar, magnetometers, underwater cameras and lidar, to perform pipeline detection and tracking [3–5]. Figure 1 shows a scenario of subsea pipeline tracking and inspection using an AUV equipped with many sensors.

To achieve real-time tracking of subsea pipelines, the AUV needs to be able to detect and locate subsea pipelines in real time and accurately. Lidar, underwater cameras, side-scan sonar and forward sonar can only detect exposed uncovered subsea pipelines and cannot detect buried subsea pipelines [6–9]. Sub-bottom profiling sonar can penetrate a certain depth of the seabed to detect buried pipelines, and when it moves perpendicular to the pipeline, it can detect the arc profile of the pipeline [10, 11]. Sub-bottom profiling sonar cannot locate the pipeline when the carrier AUV moves longitudinally along the pipeline, so it is not used to track subsea pipelines.

* Author to whom any correspondence should be addressed.

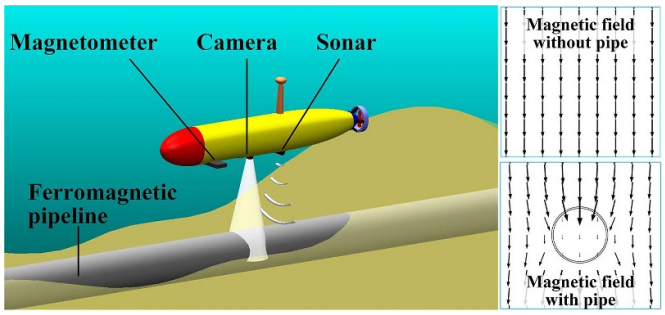

Figure 1. Pipeline detection with an AUV.

Subsea pipelines are made of low-carbon steel with very high magnetic permeability. Under the magnetization of the background geomagnetic field, magnetic anomalies can be caused near pipelines, which can be used to detect and locate them. Seawater, rock and sediment have the same magnetic permeability as air, so they do not interfere with the magnetic anomalies produced by subsea pipelines. Compared to methods of vision, lidar and sonar, magnetic methods can detect both uncovered and buried subsea pipelines without being affected by seawater turbidity. They also have low power consumption. For a long time, AUVs and surveying vessels have been equipped with magnetometers to identify subsea pipelines in an offline form. They scan the seabed over a large area, collect magnetic data at many grid points and run complex offline algorithms to identify the magnetic anomalies of subsea pipelines [12–16]. Few of these studies directly focus on real-time tracking of subsea pipelines. Nonetheless, there are still studies that are promising in this direction on aspects of magnetic anomaly modeling and pipeline location implementation schemes.

In terms of pipeline magnetic anomaly modeling, Wang *et al* [17] deduced a theoretical calculation model of the total magnetic field anomaly of subsea pipelines based on the Poisson equation and concluded that the magnetic anomaly amplitude is linearly and positively correlated with the intensity of the background magnetic field, the square difference between the outer and inner pipe diameters, and the magnetic susceptibility, but is inversely proportional to the square of the measurement plane height. Wu and Wei [18] established the magnetic anomaly model of non-coplanar cross pipelines based on the principle of magnetic dipole reconstruction and analyzed the influence of pipeline parameters, geomagnetic parameters, cross angle and other factors on the magnetic anomaly of non-coplanar pipelines. Zhao *et al* [19] also used the magnetic dipole reconstruction method to establish and analyze magnetic anomaly models of pipes with different shapes, such as straight pipes, elbows and tee joints. These models are very accurate in the ideal case without any external magnetic interference or geomagnetic parameter variance. However, in reality, this ideal situation does not exist, and when coupled with the weak magnetic anomaly signal, it is not easy to locate pipelines using these models in the field.

In order to detect and locate pipelines with magnetic anomalies, Yang *et al* [20] used the midpoint between the maximum and minimum of the gradient of the magnetic norm anomaly curve to determine the pipeline's position. However, this method is only suitable for pipelines with large and regular magnetic anomalies, manual evaluation is required, and automation cannot be realized. Li *et al* [21] proposed an iterative Tikhonov regularization method for buried pipeline location based on magnetic inclination angle and downward continuation. This requires multiple iterations to calculate the magnetic anomaly of the survey surface, which increases the time complexity. Sheinker and Moldwin [22] used the principal component analysis method to reduce the noise when using the magnetic norm anomaly to detect the pipeline, but the local geomagnetic inclination needs to be known in advance. Bharti *et al* [23] used an AUV equipped with two fluxgate sensors to calculate the magnetic norm anomalies at two points in the transverse direction to locate pipelines and used parameterized Kalman filters to track pipelines. In these studies, magnetic norm anomalies are used to determine pipeline location. An advantage of these methods is that alignment of the sensor coordinate system is not required, and a disadvantage is that the magnetic norm anomaly shape is easily changed by the geomagnetic inclination and the carrier magnetic interference. The positioning is not intuitive and accurate enough for pipeline tracking.

Magnetic component characterization and signal-to-noise ratio (SNR) enhancement are adopted by some pipeline localization methods. Guo *et al* [24] used the vertical magnetic component and its derived signals to locate a single pipe, parallel pipes and cross pipes. Its correctness and effectiveness were verified by numerical simulations. Chau *et al* [25] proposed a method to calculate the depth of the pipeline by measuring the lateral and vertical magnetic components at two points in the direction perpendicular to the pipeline using a fluxgate sensor. This method requires knowing the exact orientation of the pipeline in advance and aligning the magnetic sensor to the pipeline coordinate system. Zhao *et al* [26] used a coil array to generate an AC magnetic field containing high and low frequency components to actively magnetize a pipeline and to improve the anti-interference ability and SNR of the pipeline magnetic anomaly. Due to the rapid attenuation of AC electromagnetic waves in salty seawater, this method is not suitable for subsea pipeline detection, but does provide a new way to improve pipeline positioning accuracy.

Analysis of the state of the art above shows that it is difficult to establish an accurate pipeline magnetic anomaly model because, in the field, the angle between the pipeline orientation and the geomagnetic field is unknown. When moving magnetic surveys in the field, it is difficult to align the magnetometer/pipeline with the geomagnetic coordinate system. Magnetic norm anomalies are mostly used to locate the pipeline. The magnetic norm anomaly characteristics of the pipeline are easily affected by the magnitude and direction of the background magnetic field [13]. In addition, under the weak magnetization of the geomagnetic field, the magnetic anomaly signal of a pipeline is very weak, and the SNR is extremely low. An intuitive and reliable pipeline positioning method is needed in order to realize pipeline tracking.

This paper proposes a pipeline positioning method based on active magnetization and sensing in a single vertical direction.

Using a magnet array to locally magnetize the pipeline, the magnetic anomaly of the pipeline can be enhanced and effects of various external magnetic interferences can be suppressed, which significantly improves the SNR and ultimately makes the pipeline positioning algorithm simple, accurate and fast. However, this kind of magnetization is completely different from that when a long pipeline is immersed in an infinite space geomagnetic field. Traditional models of pipeline magnetic anomalies are no longer applicable. Therefore, this paper carries out numerous accurate finite element simulations to explore the effects of many internal and external factors, select the appropriate configuration scheme, and verify the effectiveness of active magnetization. Experiments are carried out to verify the simulation results and the advantages of local active magnetization. It is demonstrated that, through local magnetization, the magnetic anomaly characteristics of the pipeline are more noticeable, the SNR is higher, and ultimately, simple and accurate 3D positioning of the pipeline can be realized. The original magnetic data in the vertical direction measured in real time can immediately and reliably characterize the position of the pipeline, which makes real-time tracking of pipelines through magnetic detection possible.

2. Finite element simulations

2.1. Simulation configurations

The finite element simulation model is shown in figure 2. The simulation software used is COMSOL. Two rows of magnet arrays are placed above the steel pipe. The length of the magnet array is approximately three to five times the diameter of the pipe. All the N poles of the magnets are upward. The magnetometer array is placed on the measuring line or plane above the magnets. In the simulations, there is a steel pipe in the air domain with a length of $L = 20$ m and an outer diameter of d_1. The size of the air domain is 40 m × 10 m × 10 m, and its relative magnetic permeability is 1. The principle of determining the size of the air domain is that the simulation results do not change as the size increases. The pipe is horizontally laid along the x-axis. The center of the pipe is the origin of the coordinate system. The background magnetic field is the geomagnetic field $\boldsymbol{B}_\mathbf{b}$ at Tianjin, China, and $\boldsymbol{B}_\mathbf{b} = (B_{bx}, B_{by}, B_{bz}) = (16, 1.8, -39)$ (A m^{-1}). The six surfaces of the air domain containing the pipeline and the magnets are set as 'external magnetic flux density' boundary conditions. All the domains are meshed into free triangular type meshes. All domains except for the air domain, including pipe, magnet array, iron plate and measurement lamina are meshed into extremely fine meshes whose minimum mesh size is no less than 2 mm and maximum size is no more than one to three times the thickness of each part (pipe, magnet array, iron plate and measurement lamina) in the thickness/length direction. The air domain dimension is 40 m × 10 m × 10 m, and it is meshed into normally fine meshes whose minimum mesh size is no less than 70 mm and maximum size is no more than 400 mm.

A total of seven sets of simulations are carried out: (a) one magnet at different locations to show the advantage of active magnetization and the necessity of an array of magnets; (b) influences of the relative position of the magnet array and magnetic sensors; (c) comparison of with and without the magnet array; (d) influences of magnetic permeability and pipe diameter; (e) magnetic imaging of V/X shaped pipes; (f) influence of orientation angle between the magnet array and the pipeline; (g) influence of geomagnetic inclination. Each simulation scheme is described separately in the following sections.

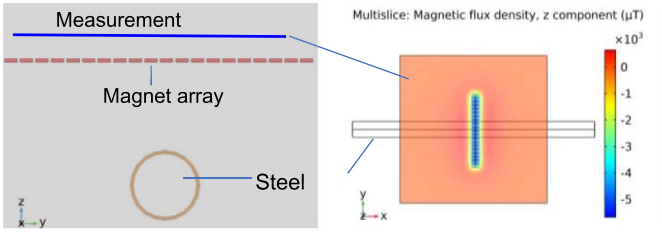

Figure 2. Simulation model.

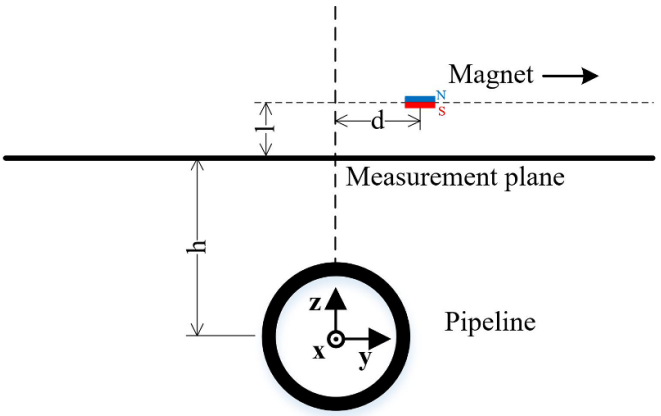

Figure 3. Simulation model schematic with one magnet moving to different positions.

2.2. Simulation results

2.2.1. One magnet at different locations. Simulations with one magnet at different locations above the pipe are carried out to analyze the active magnetization effect on the pipeline's magnetic anomaly. As shown in figure 3, a pipe is laid on the line of $y = 0$ and $z = 0$, a single magnet horizontally moves above the pipe with lateral offset d being swept, and the measurement plane is between the magnet and the pipe. The magnet dimension is 4 × 4 × 1 cm^3, $h = 0.3$ m and $d = 0$ m, 0.2 m, 0.4 m, respectively. Magnetization of the magnet is set as (0, 0, −500 000) (A m^{-1}). The observation surface is a 2.4 × 2.4 m^2 area parallel to the x–y plane with $h = 0.3$ m. Magnetic flux density component B_z is collected. The pipe is then removed and the background magnetic flux density B_{bz} is collected under the same conditions. Finally, the magnetic anomaly, B_z–B_{bz}, caused by the pipe only, is calculated. The results are shown in figure 4.

It can be seen from the left column in figure 4 that the magnet generates a bright spot on the $|B_z|$ and $|B_{bz}|$ images and the spot of $|B_z|$ with a pipe is always below the magnet no matter

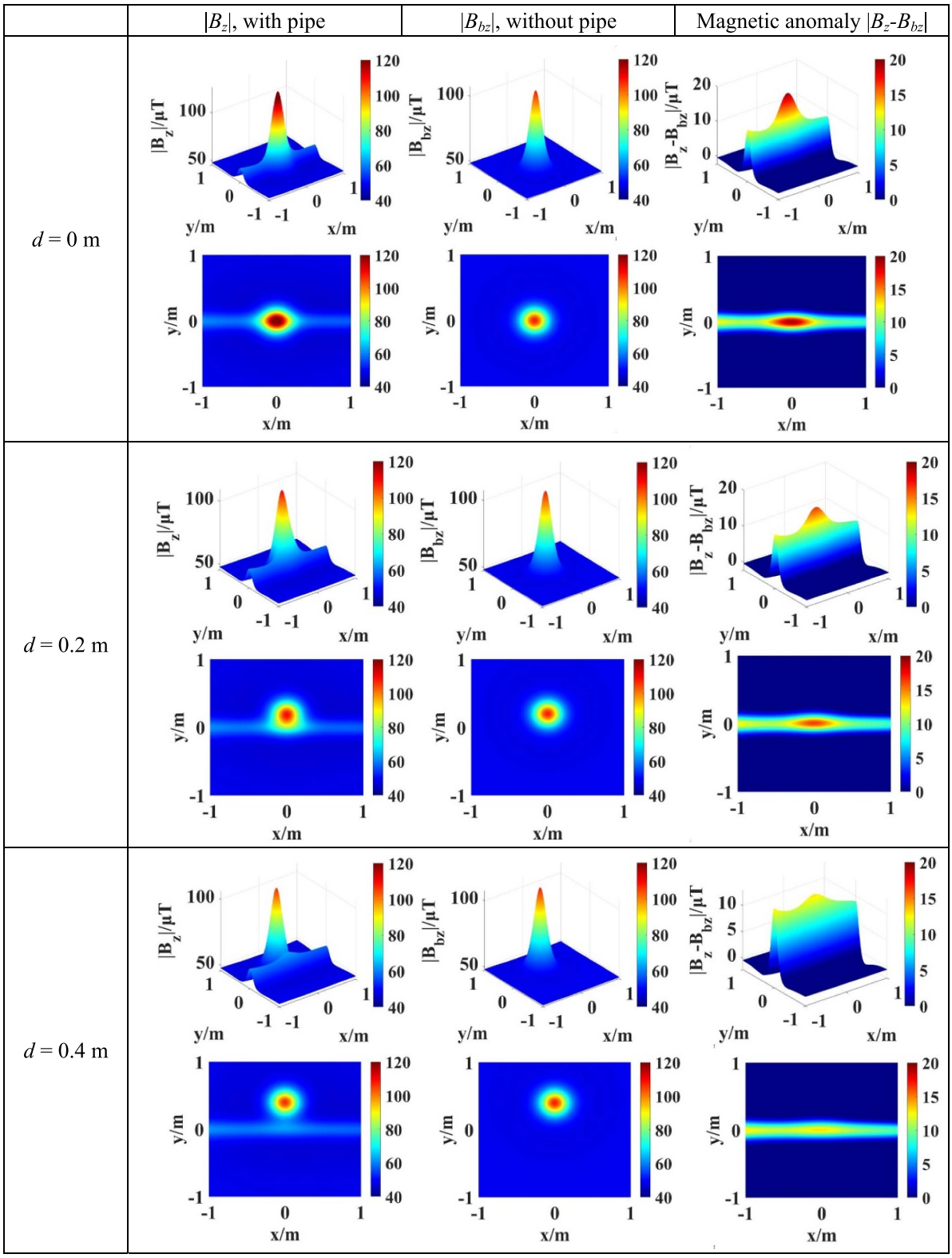

Figure 4. Magnetic flux density norms when $d = 0$ m, $d = 0.2$ m, $d = 0.4$ m. Left: $|B_z|$ generated by the magnet and the pipe, middle: $|B_{bz}|$ generated by the magnet only, right: $|B_z–B_{bz}|$ generated by the pipe.

where the magnet is. B_z alone does not adequately indicate the location of the pipe. In order to highlight the magnetic anomaly caused by the pipe, B_{bz} is subtracted from B_z, as displayed in the right column of figure 4. It can be found that the bright spot of $|B_z–B_{bz}|$ is always right above the pipe no matter how the magnet position changes. $|B_z–B_{bz}|$ can exactly indicate where the pipe is. The magnetic anomaly $|B_z–B_{bz}|$ at $x = 0$ where the magnet is located is much greater than that without the magnet,

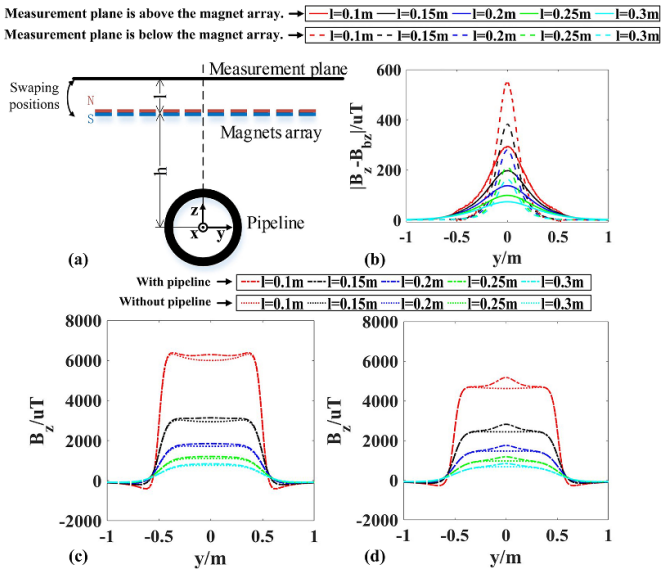

Figure 5. Magnetic anomalies with different distances between the magnet array and measurement line: (a) simulation model schematic; (b) $|B_z–B_{bz}|$; (c) B_z when the measurement plane is above the magnet array; (d) B_z when the measurement plane is below the magnet array.

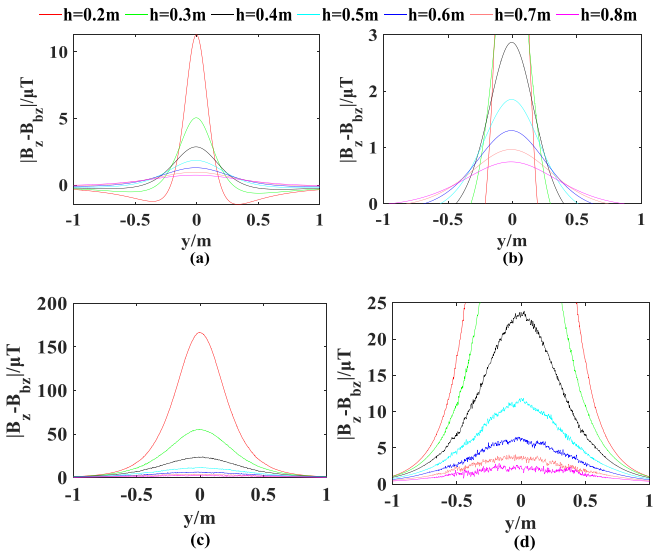

Figure 6. Magnetic anomalies at different measuring heights without and with the magnet array. (a) and (b) Without the magnet array. (c) and (d) With the magnet array. The right column shows zoomed-in views of the left column.

indicating that active magnetization is essential, and the presence of the magnet can significantly enhance the magnetic anomaly of the pipe. As the lateral distance d between the magnet and the pipe increases, the peak value of $|B_z–B_{bz}|$ gradually decreases, so multiple magnets (a magnet array) should be used in order to cover the pipe.

2.2.2. Influences of the relative position of the magnet array and magnetic sensors. In order to determine whether the magnet array should be above or below the magnetic sensor, as well as the appropriate distance between them, simulations are carried out. As shown in figure 5(a), a 2 × 20 magnet array is used and the element interval is 5 mm. h is fixed at 0.2 m and l is swept with values of 0.1 m, 0.15 m, 0.2 m, 0.25 m and 0.3 m. Two groups of simulations of swapping the magnet array and measurement plane positions are carried out. The simulation results are shown in figures 5(b)–(d).

As shown in figure 5(b), when the measurement plane is below the magnet array, the magnetic anomaly curve of $|B_z–B_{bz}|$ is higher and steeper. When the measurement plane is above the magnet array, the $|B_z–B_{bz}|$ curve is a little lower and squatter, about half the $|B_z–B_{bz}|$ curves when the measurement plane is below the magnet array. Considering that the magnetic sensors are evenly distributed along the measurement line, steeper curves are more likely to be undersampled, which may result in low-quality curve fitting and large pipeline detection errors. Therefore, deployment of the measurement plane above the magnet array is used in this paper. On the one hand, the peak values of the $|B_z–B_{bz}|$ curves become higher as the distance l between the magnetic sensors and the magnet array increases, as shown in figure 5(b); on the other hand, when l is too small, the total B_z sensed by the magnetic sensors can be very large, as shown in figures 5(c) and (d), and the magnetic sensor may saturate. l should be set to a proper value to make B_z not exceed the measurement range of the magnetic sensor employed.

2.2.3. Comparison between with and without magnet array. Simulation results with and without the magnet array are shown in figure 6. It can be seen from figures 6(a) and (b) that when a magnet is not used, as h increases from 0.2 m to 0.8 m, the peak value decreases from 11.3 μT to 0.8 μT. In the actual detection scenario, the peak value has a positive correlation with the detection sensitivity and a limited detection distance. When the peak value approaches 0, the pipe cannot be detected. Therefore, at the same distance, the greater the peak value is, the further the limit measurement distance will be.

Simulation results with the magnet array are shown in figures 6(c) and (d). It can be seen that when the magnet array is used, as h increases from 0.2 m to 0.8 m, the peak value changes from 166.3 μT to 2.4 μT. Noticeably, the magnet array greatly enhances the magnetic anomaly caused by the pipe when compared with the cases without the magnet. Another benefit of using the magnet array is that the pipeline does not need to be right below the center of the magnet array. In a certain range of lateral offset, the detection sensitivity is always high and unchanged.

2.2.4. Influence of magnetic permeability and pipe diameter. Simulations of sweeping relative magnetic permeability μ_r are carried out to study the influence of permeability, where μ_r = 10–500 and d_1 = 219 mm. The results are shown in figure 8. It can be seen that the larger μ_r is, the more noticeable the magnetic anomaly is. In order to quantitatively evaluate the magnetic anomaly, formula (1) is used to fit each curve in figure 7(a). a_1 obtained by fitting is displayed in

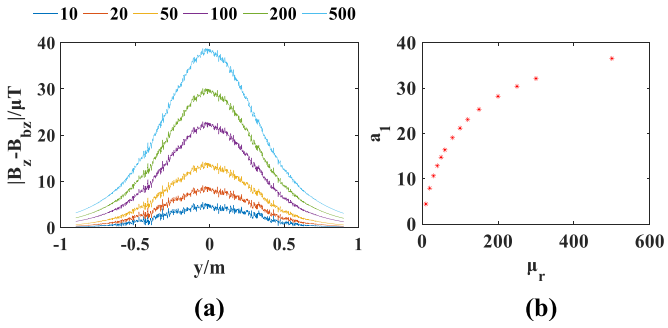

Figure 7. Influence of the relative permeability μ_r on the magnetic anomaly: (a) $|B_z–B_{bz}|$; (b) a_1 at different μ_r.

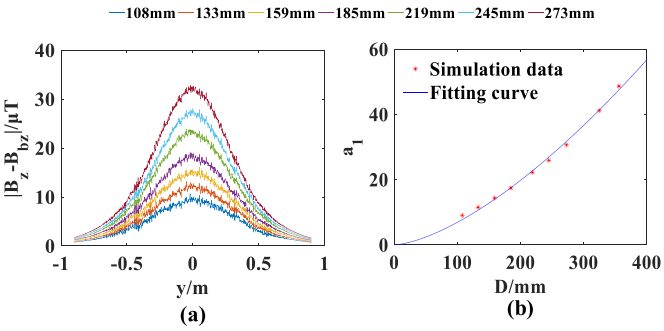

Figure 8. Magnetic anomalies of pipes with different diameters: (a) $|B_z–B_{bz}|$; (b) fitted a_1 as a function of d_1.

figure 7(b). The larger μ_r is, the less obvious the magnetic anomaly changes as μ_r changes. The relative permeability of a section of steel pipe is small and between 95 and 150 according to experimental measurement in [27]. The relative permeability of a field pipeline can be measured in advance. A magnetometer array is required to measure the transverse magnetic anomaly distribution. The difference between the magnetic signals measured by the middle magnetometers and by the magnetometers at two ends should be used to judge the existence of a pipeline,

$$\Delta B_z(y) = |B_z - B_{bz}| = a_1 * \mathrm{e}^{-((y-a_2)/a_3)^2}. \quad (1)$$

Simulation parameters of sweeping d_1 are as follows: $l_m = 3.3$ m, d_1 is swept and $d_1 \in \{108$ mm, 133 mm, 159 mm, 185 mm, 219 mm, 245 mm, 273 mm, 325 mm, 356 mm$\}$, $t = 6$ mm and $\mu_r = 110$. Simulation results are shown in figure 8(a). It can be seen that a pipe with larger diameter can cause larger magnetic anomalies of the B_z component. In order to quantitatively evaluate the magnetic anomaly of the B_z component, formula (1) is used to fit each curve in figure 8(a). a_1 obtained by fitting is displayed as star points in figure 8(b). Based on the distribution characteristics of the amplitude, a_1 vs d_1, another function of $a_1 = b_1 * d_1^{\,b_2}$ is used to fit those discrete points of a_1 vs d_1. b_1 and b_2 obtained by fitting are 0.006 28 and 1.52, and the goodness of fit R^2 is 0.9957.

2.2.5. Magnetic imaging of V/X shaped pipes. Two groups of simulations are carried out, as shown in figures 9(a)–(d). In figures 9(a) and (b), two pipes are placed on a plane to form a V-shaped with an included angle of about 30°, and their ends touch together. In figures 9(c) and (d), two pipes are placed crosswise to form a non-coplanar X shape with an included angle of about 30°. For V-shaped pipes, the geometric size is $l_m = 1$ m, $d_1 = 108$ mm and $t = 6$ mm. For X-shaped pipes, the geometric size is $l_m = 5$ m, $d_1 = 108$ mm and $t = 6$ mm. t is pipe wall thickness. The magnet array and the measurement plane are 0.2 m and 0.4 m above the pipes, respectively. These simulation configuration parameters are the same as those in the subsequent verification experiment. Simulation results are shown in figures 9(e) and (f).

It can be seen that for the V-shaped pipes when the measurement points/magnet array are on/above line 1 and line 2, the B_z component has only one peak and cannot distinguish the two pipes. When the measurement points/magnet array is on/above lines 3 and 4, the B_z component has two peaks with equal height and they can be used to determine the horizontal position and direction of the two pipes. For X-shaped pipes, when the measurement points are on lines 6, 7, and 8, the B_z component has two peaks with different heights and they can be used to determine the horizontal position and direction of the two pipes. Since the two pipes are not in the same plane, the peaks of the two magnetic anomalies are very different.

2.2.6. Influence of orientation angle between the magnet array and the pipeline. When the AUV carries the magnet array to detect and position subsea pipelines, the AUV's heading may not always be along the pipeline and the magnet array may not always be perpendicular to the pipeline. In order to study the influence of the orientation angle between the magnet array and the pipe axis on location accuracy, simulations are carried out. Under the magnetization of the magnet array in different orientations, the magnetic anomaly generated by the pipeline on the measurement line is obtained. Figure 10(a) shows the simulation model with different orientation angles, and the simulation results are shown in figure 10(b).

It is found that when θ changes from 90° to 0°, the peaks of the magnetic anomaly curves remain in the center of the measurement line, which means that the pipeline location accuracy in the horizontal plane does not deteriorate. When θ changes from 90° to 0°, the magnetic anomaly curve becomes a little thinner and its peak amplitude becomes a little lower, which may reduce the accuracy of the pipeline depth measurement. It is worth noting that when θ is between 60°–90°, namely, when the angle between the carrier (AUV) heading and the pipeline orientation is within ±30°, the magnetic anomaly curves almost coincide with each other, and the peak amplitude change is no more than 5%, which has a negligible impact on the measurement accuracy of pipeline depth. This

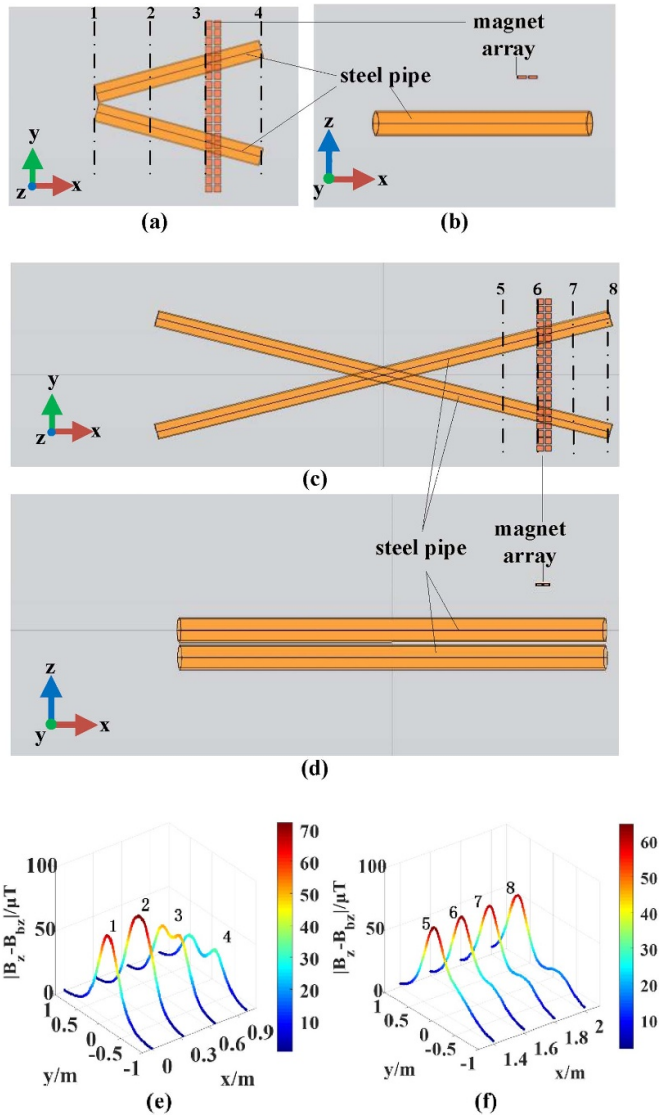

Figure 9. Magnetic imaging of V-shaped pipes: (a) vertical view of simulation model, V-shaped; (b) front view of simulation model, V-shaped; (c) vertical view of simulation model, X-shaped; (d) front view of simulation model, X-shaped; (e) $|B_z–B_{bz}|$ on lines 1, 2, 3 and 4 of simulation model, V-shaped; (f) $|B_z−B_{bz}|$ on lines 5, 6, 7 and 8 of simulation model, X-shaped.

is achievable because when the carrier (AUV) normally tracks the pipeline, the angle between them is very small and the magnet array is usually perpendicular to the pipe.

2.2.7. Influence of geomagnetic inclination I. During long-distance inspection of pipelines, the geomagnetic inclination at the location of the pipeline may change due to changes in geographic location. First, simulations are carried out to determine the influence of different geomagnetic inclinations I on the pipeline magnetic anomaly when there is no magnet, and the results are shown in figure 11(a). It can be seen that when there is no active magnetization by the magnets, the geomagnetic inclination I has a great influence on the shape of the magnetic anomaly ($|B_z−B_{bz}|$) curve of the pipeline. Magnetic anomaly curves do not have fixed features

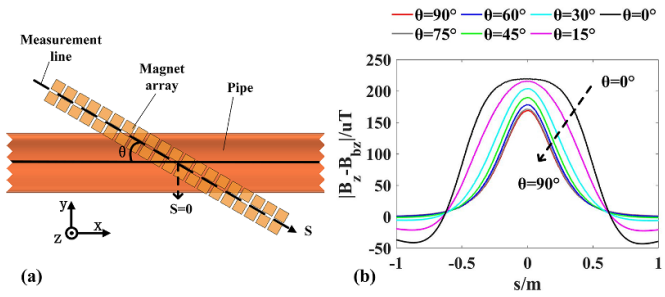

Figure 10. Magnetic anomalies of pipes with different orientation angles. (a) Vertical view of simulation model; (b) $|B_z–B_{bz}|$ at different orientation angles.

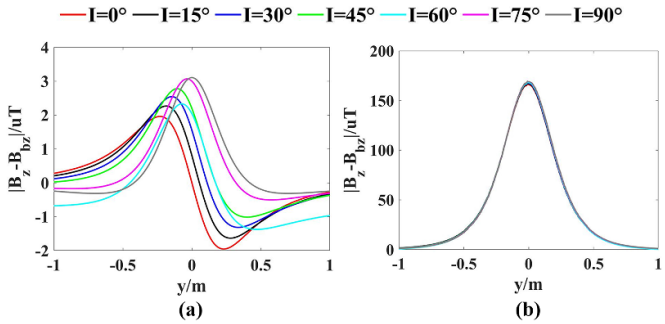

Figure 11. Magnetic anomalies with different geomagnetic inclinations. (a) $|B_z–B_{bz}|$ without magnet array; (b) $|B_z–B_{bz}|$ with magnet array.

indicating pipeline position when I changes from 0° to 90°, and different pipeline feature extraction algorithms need to be designed for different geomagnetic inclination angles, which can lead to pipe-positioning algorithms being very complex and unreliable.

For comparison, finite element simulations of magnetic anomaly distributions above the pipeline with a magnet array and with different geomagnetic inclinations are also carried out, and the results are shown in figure 11(b). It can be seen that the magnetic anomaly $|B_z−B_{bz}|$ curves almost completely overlap with each other when I changes from 0° to 90° and the peak indicating that the pipeline position remains unchanged. Due to the additional fixed magnetization by the magnet array on the pipeline, the geomagnetic inclination has no effect on the pipeline detection sensitivity or pipeline positioning accuracy of the proposed method.

3. Experiments

The experimental setup is shown in figure 12. Two rows of magnet arrays are placed above the steel pipe. The length of the magnet array is approximately three to five times the diameter of the pipe. All the N poles of the magnets are upward. Fifty magnetometers are evenly distributed directly above the magnetic array. The magnetometers are of triaxial anisotropic magnetoresistance type with a measurement range of ±16 Gs and a resolution of 0.05 μT. The sensitivity axes of

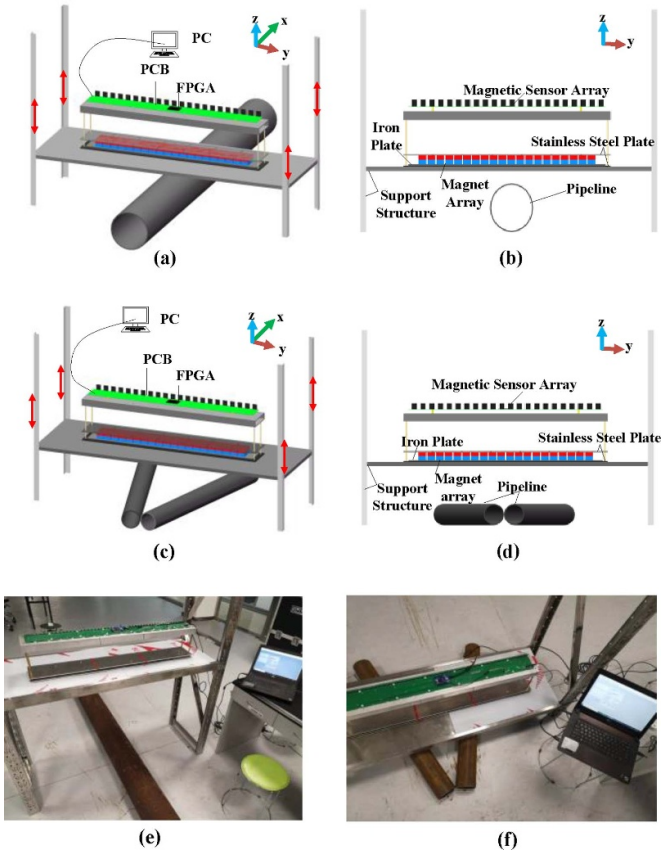

Figure 12. Experimental apparatus: (a) structural model of the long pipe, 3D view; (b) structural model of the long pipe, front view; (c) structural model of the V-shaped pipe, 3D view; (d) structural model of the V-shaped pipe, front view; (e) experiment photo of the long pipe; (f) experiment photo of the V-shaped pipe.

the magnetometer and the magnetization axis of the magnet are in the same direction. An field-programmable gate array controller is used to simultaneously collect all the 50-channel magnetic data and upload the collected data to the personal computer for storage, display and analysis. The magnet and magnetometer array is about 1 m wide and is capable of covering the Φ219 mm steel pipe below the array. The pipe used in the experiment has the same outer diameter and the same wall thickness as in the simulation. The measuring platform is supported above the pipe. The magnet array is placed horizontally above the platform, and its height can be adjusted by the copper pillars. The magnet array is adsorbed on a ferromagnetic iron plate to form a large magnet. This large magnet is clamped and fixed by two stainless steel plates. The magnetic signal acquisition device is fixed on a rectangular aluminum tube, and the aluminum tube is fixed on one of the two stainless steel plates. The magnet, iron plate, stainless steel plate, aluminum tube and magnetic signal acquisition module are connected as a whole and hung on a stainless steel bracket, and they can be moved up and down as a whole to change the lift-off value h. Detection experiments of one single straight pipe and V-shaped pipes are carried out.

4. Results and analysis

4.1. Pipeline horizontal position

When there is no magnet, B_z is measured when the lift-off value h is 0.28 m–0.73 m. Then, the pipe ias removed, and B_{bz} measured. Differential magnetic anomaly $|B_z - B_{bz}|$ was calculated in order to detect and locate the pipe. The results are shown as the star points in figures 13(a) and (b). Then the magnet array was employed. Keeping the distance between the magnet and the magnetometer constant, B_z was measured with the pipe and B_{bz} was measured without the pipe when the lift-off value h is 0.28 m–0.88 m. Differential magnetic anomaly $|B_z – B_{bz}|$ is shown as the star points in figures 13(c) and (d). Each point represents the output of a single magnetometer. Formula (1) is used to fit the experimentally measured data and the fitting curves are shown as solid curves in figures 13(a)–(d). The magnetometer interval is 20 mm and the origin of the coordinate system is at the center of the array, so y coordinate of the ith sensor is $(i\text{-}25.5)^*20$ mm.

It can be seen from the raw data that the signal dispersion is much smaller and the magnetic anomaly is much larger when there are magnets than without magnets for each lift-off value h. As h increases, the peak value of the magnetic anomaly gradually decreases and the point curve gradually becomes flat. As h increases, the pipe cannot be detected earlier in the case without magnets than in the case with magnets. It is shown that employing the magnet array greatly increases the measurement sensitivity and distance.

The SNR is calculated for quantitative comparison. First, the experimental data in figures 13(a)–(d) was fitted by the formula (1), and the magnetic anomaly peaks A and N were obtained. $A = a_1$, and N is the average residual error, which is chosen as the experimental noise amplitude. The signal is defined as $S = A - (\Delta B_z(-0.4) + \Delta B_z(0.4))/2$, and S is the magnetic anomaly amplitude caused by the pipeline. The SNR is calculated as follows: $\mathrm{SNR} = 20\log10(S/N)$. As shown in figure 13(e), the SNR goes down as the lift-off value h goes up. For each h, the SNR of the scheme with magnets is much higher than that of the scheme without magnets, and the SNR is improved by 5 dB–20 dB. The lateral pipe positioning error of the scheme with magnets (−0.03–0.03 m) is much smaller than that of the scheme without magnets (−0.05 m to −0.17 m), as shown in figure 13(f). It has been experimentally demonstrated that active magnetization with the magnet array cannot only enhance the sensitivity of pipe detection, but also improve pipeline positioning accuracy.

4.2. Pipeline depth

Using a magnet array to locally magnetize the pipeline is completely different from the magnetization model of a long pipeline in an infinite space geomagnetic field. Traditional models of pipeline magnetic anomalies regarding pipeline depth and location are no longer applicable to the proposed

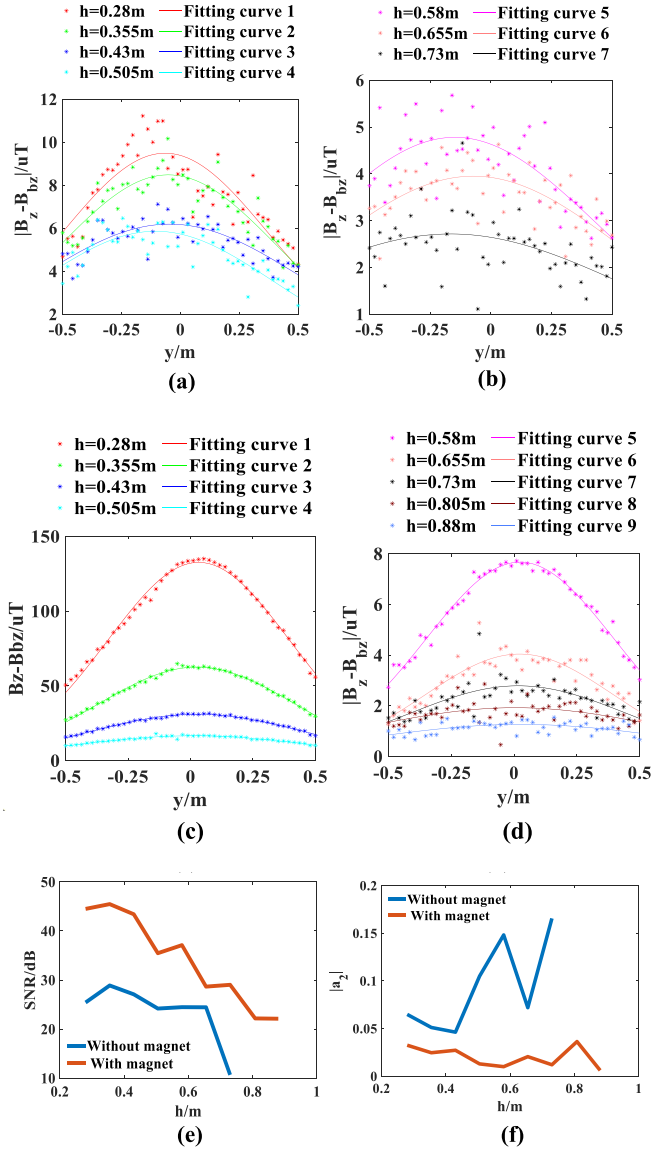

Figure 13. Pipe detection result comparison of the two schemes: (a) without the magnet array, $h = 0.28$ m, 0.355 m, 0.43 m and 0.505 m; (b) without the magnet array, $h = 0.58$ m, 0.655 m and 0.73 m; (c) with the magnet array, $h = 0.28$ m, 0.355 m, 0.43 m and 0.505 m; (d) with the magnet array, $h = 0.58$ m, 0.655 m, 0.73 m and 0.805 m and 0.88 m; (e) SNR at different heights; (f) a_2 at different heights.

magnetization scheme. Since the pipe diameter, pipe wall thickness, pipe magnetic permeability and magnetic field of the magnet can all be known in advance, we can obtain the empirical formula between the pipeline magnetic anomaly characteristic parameters and pipeline depth through accurate finite element simulations. Finally, the pipeline depth can be calculated via substituting the measured magnetic anomaly parameters into the empirical formula.

Formula (1) is used to fit the magnetic anomaly curves of pipelines with different depths obtained by simulation, where $y = h + l$, to obtain the characteristic parameter a_1 at different $h + l$. Simulation data of ΔB_z (y) used for fitting are shown in

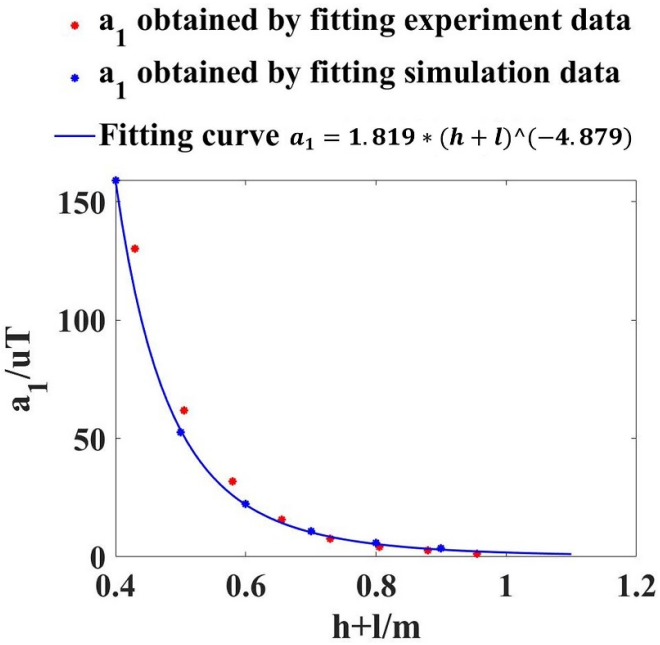

Figure 14. A_1 vs $h + l$ with different pipeline depths.

Table 1. Measurement error of pipeline depth.

Measured depth (m)	Actual depth (m)	Relative error
0.417	0.430	3.07%
0.486	0.505	3.86%
0.556	0.580	4.09%
0.643	0.655	1.86%
0.745	0.730	1.99%
0.849	0.805	5.47%
0.916	0.880	4.09%
1.077	0.955	12.75%

figure 14. Then, the inverse proportional function, power function and smooth spline function are used to fit $a_1 = f(h + l)$. Among them, the power function has the best fitting effect with the fitting determination coefficient $R^2 = 0.99$. Finally, the empirical formula between a_1 and the pipeline depth $h + l$ is obtained, which is $a_1 = 1.819 \times (h + l)^{-4.879}$.

The same formula (1) is used to fit the experimentally measured magnetic anomaly curves to obtain the experimental a_1, and the result is shown in figure 14. It is shown that the experimental results are in good agreement with the empirical formula obtained by the simulation. The a_1 obtained from the experiment is substituted into this formula, and then the depth of the pipeline is calculated. The results are shown in table 1. When the depth is within 1 m, the relative error is small, less than 6%. With an increase of $h + l$, the small change of the magnetic anomaly has an influence on the calculation accuracy of the pipeline depth, whose error is about 12%. The results confirm that the pipeline depth can be simply and accurately measured by actively magnetizing the pipeline with an array of magnets.

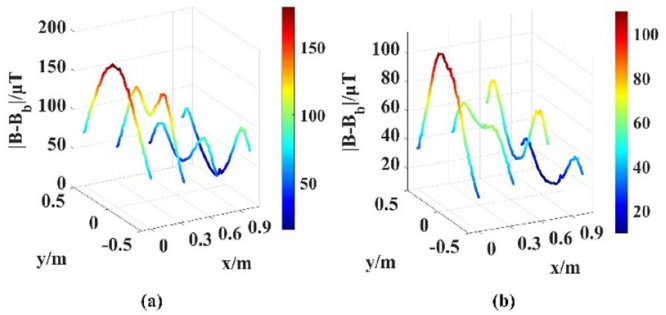

Figure 15. Experimental results of magnetic imaging of V-shaped pipes. (a) With magnet array; (b) without magnet array.

4.3. Inspection of pipes with different shapes

Finally, the proposed method is used to detect the V-shaped pipes shown in figure 12(f), and the results are shown in figure 15. When the measurement line is near the tip of the V-shaped pipes, the measured magnetic anomaly curve has only one peak and the two pipes cannot be distinguished. As the measurement line moves far away from the tip, two detected peaks appear and they become more and more noticeable. The proposed method can realize magnetic imaging of crossed V-shaped pipes. It is noted that when this scheme is equipped onto an underwater AUV, because the moving speed is slow, the electromagnetic induction is small and the magnetic field around the pipeline changes slowly, which has little impact on the measurement of pipeline magnetic anomaly and position.

5. Conclusion

This paper proposes a method capable of immediately and accurately locating pipelines via active local magnetization by a magnet array and also reveals the advantages of extra magnetization, the necessity for an array of magnets and improved anti-interference through finite element simulations and experiments. The following conclusions are reached:

(a) The magnet array can effectively improve the sensitivity and measurement distance of pipeline magnetic detection, eliminate the influence of geomagnetic inclination on pipeline magnetic anomalies, and achieve magnetic detection of pipelines of different shapes. Via local magnetization, only a single vertical magnetic component is required and the pipeline positioning algorithm is simple, accurate and fast.
(b) The detected peak position of the pipeline magnetic anomaly is used to locate the horizontal position of the pipeline. The results show that the horizontal positioning error of the pipeline is reduced under the action of the magnet array. The maximum lateral pipe positioning error of the scheme with magnets is 0.03 m and much smaller than that without magnets.
(c) The detected peak amplitude of the pipeline magnetic anomaly is used to locate the pipeline depth. The results show that the pipeline depth and the peak amplitude of the pipeline magnetic anomaly under the magnetization of the magnet array satisfy the function formula $a_1 = a^*\text{depth}^b$, which is simple and effective to calculate the pipeline depth.
(d) The magnet array can significantly increase the detection SNR. When the magnet array is employed, the influence of environmental noise is reduced thanks to the magnetization effect of the magnet array on the pipeline, the SNR is improved by 5 dB–20 dB.

Data availability statement

All data that support the findings of this study are included within the article (and any supplementary files).

Acknowledgment

This work is supported by National Natural Science Foundation of China (No. 62073233).

ORCID iDs

Xinjing Huang https://orcid.org/0000-0002-8964-8502
Jinyu Ma https://orcid.org/0000-0003-1509-9421
Hao Feng https://orcid.org/0000-0003-1552-0976

References

[1] Rumson Alexander G 2021 The application of fully unmanned robotic systems for inspection of subsea pipelines *Ocean Eng.* **235** 109214
[2] Min Y *et al* 2015 Discussion methods of buried submarine pipeline detection and application of new technology *Mar. Sci.* **39** 129–32
[3] Jacobi M and Karimanzira D 2015 Multi sensor underwater pipeline tracking with AUVs *Oceans-St. John's Conf. Fraunhofer IOSB-AST*
[4] Akram W and Casavola A 2021 A visual control scheme for AUV underwater pipeline tracking *2021 IEEE Int. Conf. on Autonomous Systems (ICAS)* (IEEE)
[5] Bharti V, Lane D and Wang S 2018 Robust subsea pipeline tracking with noisy multibeam echosounder *IEEE/OES Autonomous Underwater Vehicle Workshop* (Edinburgh Centre for Robotics, Heriot Watt University)
[6] Huang X, Gong J, Chen P, Tian Y and Hu X 2021 Towards the adaptability of coastal resilience: vulnerability analysis of underground gas pipeline system after hurricanes using LiDAR data *Ocean Coast. Manag.* **209** 105694
[7] Zhou Z *et al* 2018 Autonomous underwater pipeline tracking control based on visual images *2018 IEEE Int. Conf. on Robotics and Biomimetics (ROBIO)* (IEEE)
[8] Lai X *et al* 2011 Application of side sweep sonar system in submarine pipeline detection *Ocean Eng.* **29** 117–21
[9] Zhang Y, Zhang H, Liu J, Zhang S, Liu Z, Lyu E and Chen W 2022 Submarine pipeline tracking technology based on AUVs with forward looking sonar *Appl. Ocean Res.* **122** 103128
[10] Li S, Zhao J, Zhang H and Zhang Y 2022 Automatic detection of pipelines from sub-bottom profiler sonar images *IEEE J. Ocean. Eng.* **47** 417–32

[11] Zheng G, Zhao J, Li S and Feng J 2021 Zero-shot pipeline detection for sub-bottom profiler data based on imaging principles *Remote Sens.* **13** 4401
[12] Huang X, Jin C and Jian L 2019 Susceptibility inversion of near-field magnetic sources and its application *J. Magn. Magn. Mater.* **490** 165547
[13] Chen S *et al* 2019 An accurate localization method for subsea pipelines by using external magnetic fields *Measurement* **147** 106803
[14] Wang Y, Han Q, Zhao G, Li M, Zhan D and Li Q 2022 A deep neural network based method for magnetic anomaly detection *IET Sci. Meas. Technol.* **16** 50–58
[15] Sun T, Wang X, Wang J, Yang X, Meng T, Shuai Y and Chen Y 2022 Magnetic anomaly detection of adjacent parallel pipelines using deep learning neural networks *Comput. Geosci.* **159** 104987
[16] Wu P and Guo Z 2020 High-precision inversion of buried depth in urban underground iron pipelines based on AM-PSO algorithm for magnetic anomaly *Prog. Electromagn. Res.* C **100** 17–30
[17] Wang F *et al* 2019 Magnetic anomalies of submarine pipeline based on theoretical calculation and actual measurement *IEEE Trans. Magn.* **55** 1–10
[18] Wu P and Wei M 2020 Analysis of magnetic anomaly characteristics of underground non-coplanar cross-buried iron pipelines *J. Environ. Eng. Geophys.* **25** 223–33
[19] Zhao D, Guo Z, Du J, Liu Z, Xu W and Liu G 2020 Geometric modeling of underground ferromagnetic pipelines for magnetic dipole reconstruction-based magnetic anomaly detection *Petroleum* **6** 189–97
[20] Yang X *et al* 2019 Research on magnetic detection technology of submarine pipeline *Mar. Surv. Mapp.* **39** 52–56
[21] Li C *et al* 2020 The positioning of buried pipelines from magnetic data *Geophysics* **85** 111–20
[22] Sheinker A and Moldwin M B 2016 Magnetic anomaly detection (MAD) of ferromagnetic pipelines using principal component analysis (PCA) *Meas. Sci. Technol.* **27** 045104
[23] Bharti V, Lane D and Wang S 2020 A semi-heuristic approach for tracking buried subsea pipelines using fluxgate magnetometers *2020 IEEE 16th Int. Conf. on Automation Science and Engineering (CASE)* (IEEE)
[24] Guo Z, Liu D, Pan Q, Zhang Y, Li Y and Wang Z 2015 Vertical magnetic field and its analytic signal applicability in oil field underground pipeline detection *J. Geophys. Eng.* **12** 340–50
[25] Vo C K, Staples S G H, Cowell D M J, Varcoe B T H and Freear S 2020 Determining the depth and location of buried pipeline by magnetometer survey *J. Pipeline Syst. Eng. Pract.* **11** 04020001
[26] Zhao Y, Wang X, Sun T, Chen Y, Yang L, Zhang T and Ju H 2021 Non-contact harmonic magnetic field detection for parallel steel pipeline localization and defects recognition *Measurement* **180** 109534
[27] Xinjing H, Shan L, Zhoumo Z and Jian L 2019 Magnetic permeability measurement for steel pipe immersed in geomagnetic field *J. Magn. Magn. Mater.* **491** 165621